



HAL
open science

Characterising the transient response of CFRP/Al HC spacecraft structures induced by space debris impact at hypervelocity

S. Ryan, F. Schäfer, M. Guyot, S. Hiermaier, M. Lambert

► **To cite this version:**

S. Ryan, F. Schäfer, M. Guyot, S. Hiermaier, M. Lambert. Characterising the transient response of CFRP/Al HC spacecraft structures induced by space debris impact at hypervelocity. *International Journal of Impact Engineering*, 2008, 35 (12), pp.1756. 10.1016/j.ijimpeng.2008.07.071 . hal-00542569

HAL Id: hal-00542569

<https://hal.science/hal-00542569>

Submitted on 3 Dec 2010

HAL is a multi-disciplinary open access archive for the deposit and dissemination of scientific research documents, whether they are published or not. The documents may come from teaching and research institutions in France or abroad, or from public or private research centers.

L'archive ouverte pluridisciplinaire **HAL**, est destinée au dépôt et à la diffusion de documents scientifiques de niveau recherche, publiés ou non, émanant des établissements d'enseignement et de recherche français ou étrangers, des laboratoires publics ou privés.

Accepted Manuscript



Title: Characterising the transient response of CFRP/Al HC spacecraft structures induced by space debris impact at hypervelocity

Authors: S. Ryan, F. Schäfer, M. Guyot, S. Hiermaier, M. Lambert

PII: S0734-743X(08)00155-3

DOI: [10.1016/j.ijimpeng.2008.07.071](https://doi.org/10.1016/j.ijimpeng.2008.07.071)

Reference: IE 1637

To appear in: *International Journal of Impact Engineering*

Received Date:

Revised Date:

Accepted Date:

Please cite this article as: Ryan S, Schäfer F, Guyot M, Hiermaier S, Lambert M. Characterising the transient response of CFRP/Al HC spacecraft structures induced by space debris impact at hypervelocity, *International Journal of Impact Engineering* (2008), doi: 10.1016/j.ijimpeng.2008.07.071

This is a PDF file of an unedited manuscript that has been accepted for publication. As a service to our customers we are providing this early version of the manuscript. The manuscript will undergo copyediting, typesetting, and review of the resulting proof before it is published in its final form. Please note that during the production process errors may be discovered which could affect the content, and all legal disclaimers that apply to the journal pertain.

Characterising the transient response of CFRP/Al HC spacecraft structures induced by space debris impact at hypervelocity

S. Ryan^{*1,2}, F. Schäfer¹, M. Guyot³, S. Hiermaier¹, M. Lambert⁴

¹Fraunhofer-Institut für Kurzzeiddynamik, Ernst-Mach-Institut (EMI), Eckerstr. 4, D-79014 Freiburg, Germany

²School of Aerospace, Mechanical & Manufacturing Engineering, RMIT University, GPO Box 2476V, Melbourne, Australia

³EADS Astrium SAS, 31 rue des Cosmonautes, 31402 Toulouse Cedex 4, France

⁴ESA-ESTEC, Postbus 299, NL-2200 AG Noordwijk, The Netherlands

Abstract

To quantify the disturbance induced by the impact of micrometeoroid and space debris particles at hypervelocity on vibration-sensitive CFRP/Al HC SP satellite platforms a method is presented which uses experimentally-validated hydrocode models to characterize the impact-induced transient wave in the local structure. Key features of the transient waveform are simplified by a mathematical function which is expressed in terms of impactor momentum. Evolution of the transient waveform is characterized using multiple measurement gauges located on the sandwich panel facesheets outside the area of mechanical damage. The characterization is then used to extrapolate the elastic waveform back to the impact location. The elastic equivalent excitation of a CFRP/Al HC SP is defined in terms of force with respect to time for application in finite element structural codes for propagation of the local disturbance to vibration-sensitive locations (i.e. measurement devices).

Keywords: Hypervelocity impact, Space debris, Hydrocode, Composites

1. Introduction

The next generation of European satellites will employ ultra-high sensitivity equipment which require platform stability orders of magnitude higher than those of previous missions, e.g. ESA's Global Astrometric Interferometer for Astrophysics (GAIA) [1]. As a result, sandwich panels with carbon fiber reinforced plastic facesheets and aluminum honeycomb cores (CFRP/Al HC SP) are foreseen as the predominant platform type due to the enhanced structural benefits they provide over simple monolithic metal structures (high stiffness, low thermal expansion, etc). During the operational lifetime of these satellites, impact of micrometeoroid and space debris particles (M/SD) will induce local disturbance waves that propagate throughout the structure, leading to a possible degradation of measurement accuracy and thus preventing successful fulfillment of mission objectives.

*Corresponding author. Tel.: +49 761 2714-402; fax: +49 761 2714-316

Email address: shannon.ryan@emi.fhg.de

GAIA will operate in a Lissajous orbit about the Earth-Sun L2 point, at which the primary debris environment consists of natural, micro-sized particles traveling at velocities over 20 km/s. As such, in-orbit impact conditions cannot be reproduced in laboratory experiments, and numerical simulations are required to characterize the transient structural response. Structural finite element analysis (FEA) codes (e.g. NASTRAN) are the preferred engineering tool for investigating the response of structures under static and dynamic loading. However, considering that there are three orders of magnitude variance between the dimensions of the satellite and common impactor (m vs. μm), simulation of the entire satellite structure is not feasible in terms of the required computational time and cost. Furthermore, structural analysis codes are not suited for simulation of such extreme high loading-rate events.

Hydrodynamic computer codes, or hydrocodes, are based on explicit finite difference, finite volume, and finite element techniques and use classical continuum mechanics to describe the dynamics of a continuous media. They enable coupling of complex material models with a fluid-structure program that is ideal for simulation of highly dynamic events, particularly those involving shock wave propagation. Additionally, recent advancements [2-4] in the modeling of composite materials within the commercial hydrocode AUTODYN [5] provide an improvement over existing capabilities by allowing the description of orthotropic constitutive behavior, non-linear equation of state, orthotropic non-linear hardening, and individual material plane interactive failure initiation criteria. In the absence of experimentally-characterized composite material data a number of widely accepted and validated composite and shock mechanics theories can be used, in conjunction with generalized material properties, to derive a complete material data set from freely available constituent properties [6].

In this paper a procedure has been developed which uses experimentally-validated hydrocode numerical models to derive the elastic-equivalent excitation of a CFRP/Al HC SP (representative of those used onboard GAIA) induced by micrometeoroid impact at hypervelocity. This function provides the simplification of a hypervelocity impact process which is suitable for application in structural engineering codes (such as FE) for full scale quantification of the disturbance severity.

2. Methodology

Hypervelocity impact (HVI) of M/SD particles induces transient disturbances in satellite structures which can eventually propagate to areas of critical stability, e.g. measurement devices. Considering the impact process, a high amplitude shock wave is initially generated at the impact location, causing plastic deformation (e.g. cratering) in the front surface of the target. As the shock wave propagates into the surrounding structure, this plastic wave is rapidly dampened out, evolving into an elastic wave. At the impact site, the excitation of the panel is expected to be a single pulse in the flight direction of the projectile with a peak induced velocity in the same order of magnitude as that of the impacting projectile. At the excitation maxima, the projectile will have either perforated or been stopped by the CFRP sheet, and therefore the panel will return to rest. Given the complexity of the problem, it is not possible to calculate the panel response from 1st principles. A best approximation of this type of behavior is given by a polynomial-exponential decay function of the form:

$$V(t) = A \cdot (t - t_0)^2 \cdot e^{-\beta(t-t_0)} \quad (1)$$

Equation (1) defines a state initially at rest. Following arrival of the transient signal ($t = t_0$) the velocity increases at a rate defined by the constant A until reaching a maxima at $t = 2/\beta$. The velocity then progressively decreases at a rate defined by the constant β , finally asymptoting at $V = 0$. This provides a reasonable representation of the ideal excitation pulse induced by HVI.

To characterize the elastic excitation of the impacted structure, numerical simulations are performed in which a series of disturbance measurements are made at intervals away from the impact site where the disturbance is purely elastic. The measured elastic waveforms can then be used to characterize the evolution of the disturbance waveform in terms of distance from the impact axis. This characterization can then be extrapolated back to the impact site to define the initial elastic excitation. For example, if we know how the disturbance appears at say 4, 6, 8 and 10mm from the impact site, we can see how it changes with propagation distance and use this understanding to predict the original elastic excitation. Repeating the characterization procedure for multiple impact conditions (varying projectile diameter and impact velocity), the elastic excitation waveform can then be characterized in terms of impactor momentum, and a generalized elastic-equivalent excitation function can be defined for a specific structure impacted by debris at hypervelocity.

The nature of the induced excitation is considered to be dependant on the type of penetration and failure mechanisms caused by the impact event. Four penetration conditions are considered which are expected to induce significantly different types of disturbances in a sandwich panel structure:

1. Non-penetration case: projectile does not penetrate the outer facesheet of the SP;
2. Penetration case 1: projectile penetrates the front facesheet and is stopped inside the SP;
3. Penetration case 2: projectile minimally penetrates the SP;
4. Penetration case 3: projectile penetrates the SP completely.

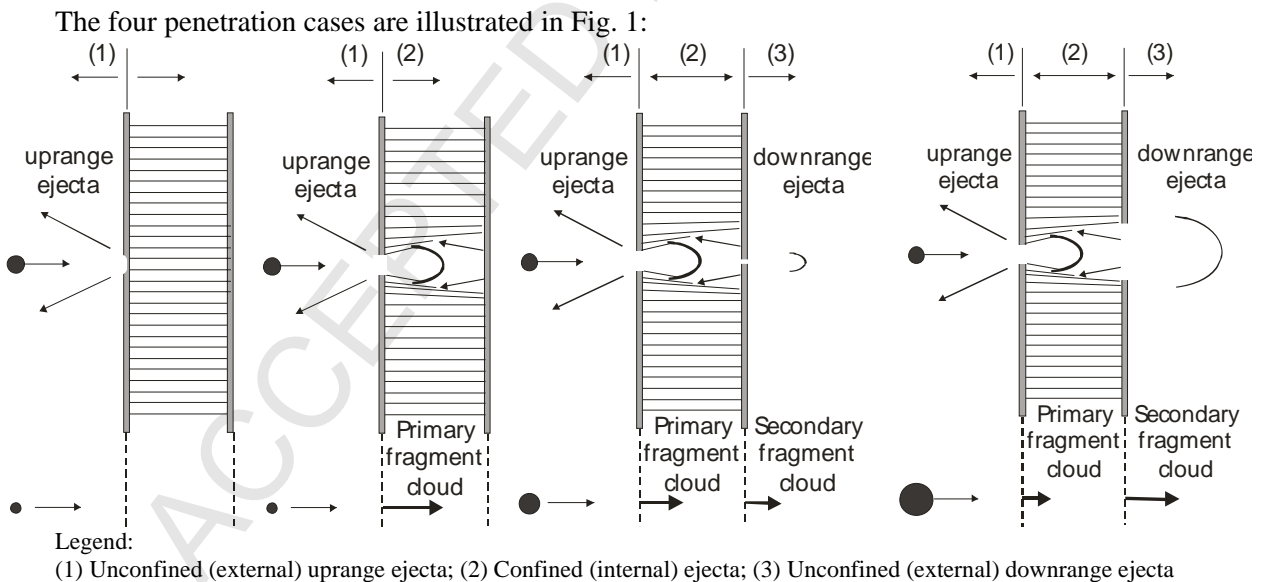


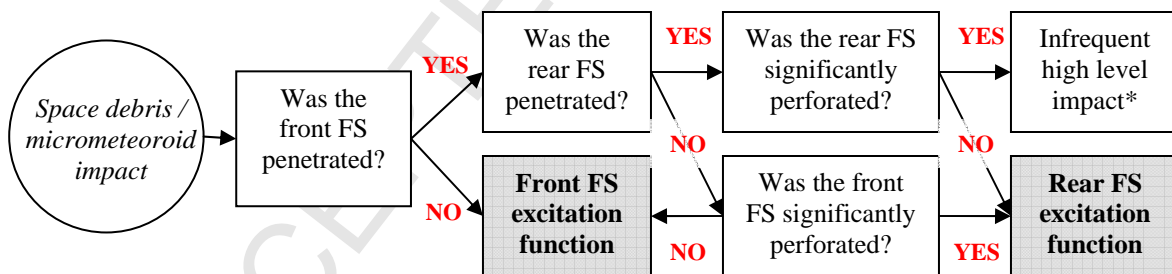
Fig. 1. Penetration phenomena of the four cases considered for impact on a honeycomb sandwich.

Each of the penetration cases results in a different energy transformation and momentum transfer condition. For the non-penetrating case, all elastic energy imparted to the sandwich panel will be realized in the front facesheet. In penetration case 1, following perforation of the front facesheet, the fragment cloud propagates through the honeycomb core, eventually impacting on the rear facesheet. At the onset of front facesheet perforation, the momentum of the perforated fragments will be low, and as such the excitation will be confined mostly to the front facesheet. As the degree of perforation increases (i.e. as the penetration approaches case 2) the projectile will show an increasing “punch-out” type perforation of the front facesheet as a result of an increasing energy overload. In this case, the response of the front facesheet will reduce, and the majority of the excitation will now occur in the rear facesheet. In this context, minimal perforation refers to the state in which an increase in projectile momentum will correspond to an increase in momentum transfer and therefore excitation of the respective perforated facesheet.

As the sandwich panel (i.e. rear facesheet) is perforated, the behavior described for perforation of the front facesheet will be repeated. At low levels of perforation (i.e. penetration case 2), the majority of projectile kinetic energy will still be imparted on the rear facesheet. As the size (and thus lethality) of the projectile increases (i.e. approaches penetration case 3), the majority of impactor kinetic energy will be ejected from the sandwich panel within the fragment cloud.

The disturbance is defined as the transient waveform induced by impact. As such, for characterization of a sandwich panel structure, the motion of the test body will not be rigid and therefore the impact-induced excitation will vary depending on the measurement location (i.e. front facesheet or rear facesheet). It is considered that the facesheet upon which the highest amplitude disturbance is induced represents the critical excitation case. Thus, for impacts which induce transient disturbances in both facesheets, only the facesheet upon which the most elastic energy is imparted will be considered for characterization.

The methodology used to define which excitation function shall be applied for a specific impact condition is shown in Fig. 2.

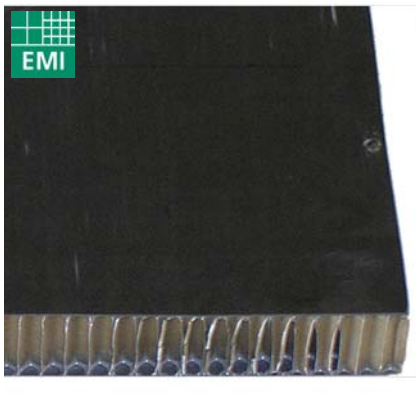


* High level (infrequent) impacts are not considered in the excitation function

Fig. 2. Methodology for application of the excitation function.

3. Numerical Simulation of Hypervelocity Impact-Induced Disturbance Propagation

Numerical simulations will be used to derive the excitation function for impact on a GAIA-representative CFRP/Al HC SP. To ensure accuracy of the numerical results, validation of the model is performed via comparison with experimentally-measured disturbance signals at achievable impact conditions (using EMI's two-stage light-gas guns [7]). Details of the experimental set-up can be found in [8]. A CFRP/Al HC SP representative of those used onboard the GAIA SVM and PLM was selected for testing, details of which are given in Fig. 3. Numerical simulations were performed in AUTODYN using volumetric elements in the SP facesheets and shell elements for the HC core foils. In the absence of experimentally-characterized material data, a procedure was applied [6] which uses a number of composite mechanics theories (e.g. micromechanics, classical laminate theory, etc.) and impact theories (e.g. Rankine-Hugoniot shock jump condition) to derive a coarse material data set from constituent (fiber and matrix) properties for application with the advanced non-linear orthotropic model for composites described in [2][3]. Details of numerical material models are given in the Appendix.



Parameter	Value	Comments
CFRP skin		
Density	1.48-1.56 g/cm ³	Measured at EMI
Thickness	0.5mm	u.d. plies
Stacking	[0°/45°/90°/-45°]	Quasi-isotropic
Fiber	M55J HM carbon	Supplier: Toray
Resin	XU 3508 (hardener 3473)	Supplier: Huntsman
Al HC core		
Designation	CRIII 3/16-5056-.0007P	Supplier: Hexcel
Thickness	20mm	-

Fig. 3. Structural details of the representative GAIA CFRP/Al HC sandwich panel selected for testing.

In Fig. 4 a comparison between the experimental and numerical disturbance signal induced by impact of a 1.5mm Al-sphere at 5.69 ± 0.07 km/s, measured on the rear side of the CFRP/Al HC sandwich panel at 50mm offset from the shot axis, is shown. The numerical signal shows good qualitative agreement with the experimental signal, capturing both the initial high-frequency disturbance and the later ($> 30 \mu\text{s}$) high-amplitude, low-frequency feature. The disturbance waveform can be separated into three distinct phases corresponding to different types of wave phenomena, namely: longitudinal, shear, and flexural. For impact tests on metallic targets, these phenomena are clearly separable and identifiable [9]; however for composite sandwich panels the distinction is more ambiguous. Nonetheless, in Fig. 4 the low amplitude pulse beginning $\sim 35 \mu\text{s}$ after impact is clearly identified as the flexural wave. It is considered that this feature of the disturbance signal is of critical importance in quantifying the effects of space debris impact-induced disturbances. Indeed, as the excitation waveform will be implemented in a structural code (maximum of the valid frequency range ~ 500 Hz), only the low-frequency section of the waveform is relevant (i.e. flexural wave). Although the propagation velocity is approximately 20% slower, the amplitude and frequency of the flexural wave is sufficiently reproduced in the numerical model.

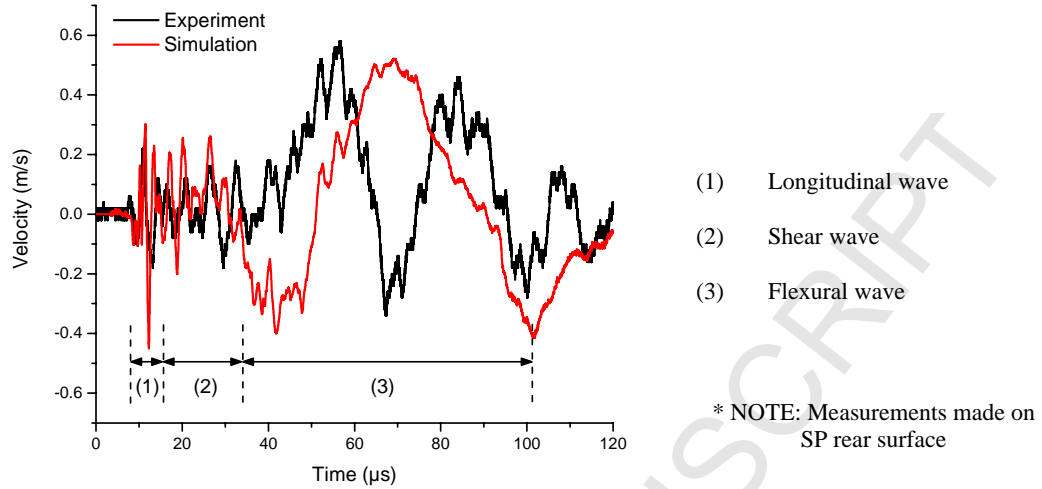


Fig. 4. Comparison of experimental and numerical signals for impact of a 1.5mm Al-projectile at 5.69 ± 0.07 km/s

4. Derivation of the Excitation Function

To characterize how the elastic waveform evolves, a series of measurements are made on the SP facesheets outside the area of plastic damage. In Fig. 5, the numerical setup (showing measurement points) and an example of waveform simplification is shown for a measurement made on the SP rear facesheet 10 mm from the impact axis. It can be noted that the polynomial-exponential decay function approaches infinity when $t < t_0$. However, as the waveform is characterized for extrapolation back to the impact site, at which $t_0 = 0$, the rapid increase of velocity for times $< t_0$ is not considered.

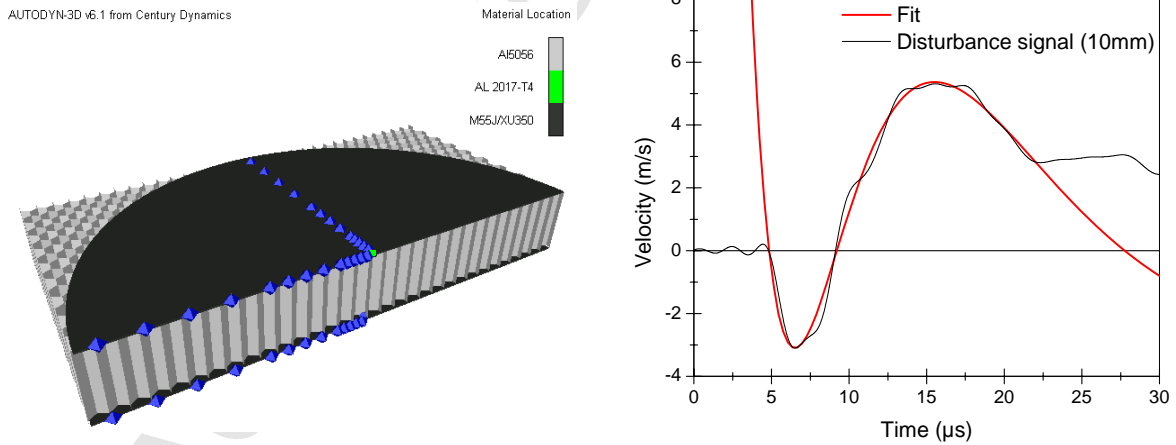


Fig. 5. Characterization of the transient disturbance. Left: Numerical model with measurement gauges; Right: Simplification of the waveform 10 mm from the impact site (SP rear side measurement)

The evolution of the flexural wave can be characterized in terms of the constants in Eqn. (1), as

shown in Fig. 6 for the specific case of a 0.6 mm Al-sphere impacting at 16.0 km/s. Extrapolation of the constants to the excitation origin can be performed, from which the original elastic excitation pulse is determined. It can be observed in Fig. 6 that constant t_0 does not trend to the origin at $x=0$ mm. This indicates that the excitation signal measured on the rear facesheet is not induced by a point-source impact, but rather a finite area with radius defined by the intercept of the t_0 linear trend.

In Fig. 6 the simplified waveforms are shown along with the extrapolated initial elastic disturbance signal. The disturbance decreases in amplitude as it propagates from the impact location, while the frequency of the increases and the acceleration rate becomes progressively slower.

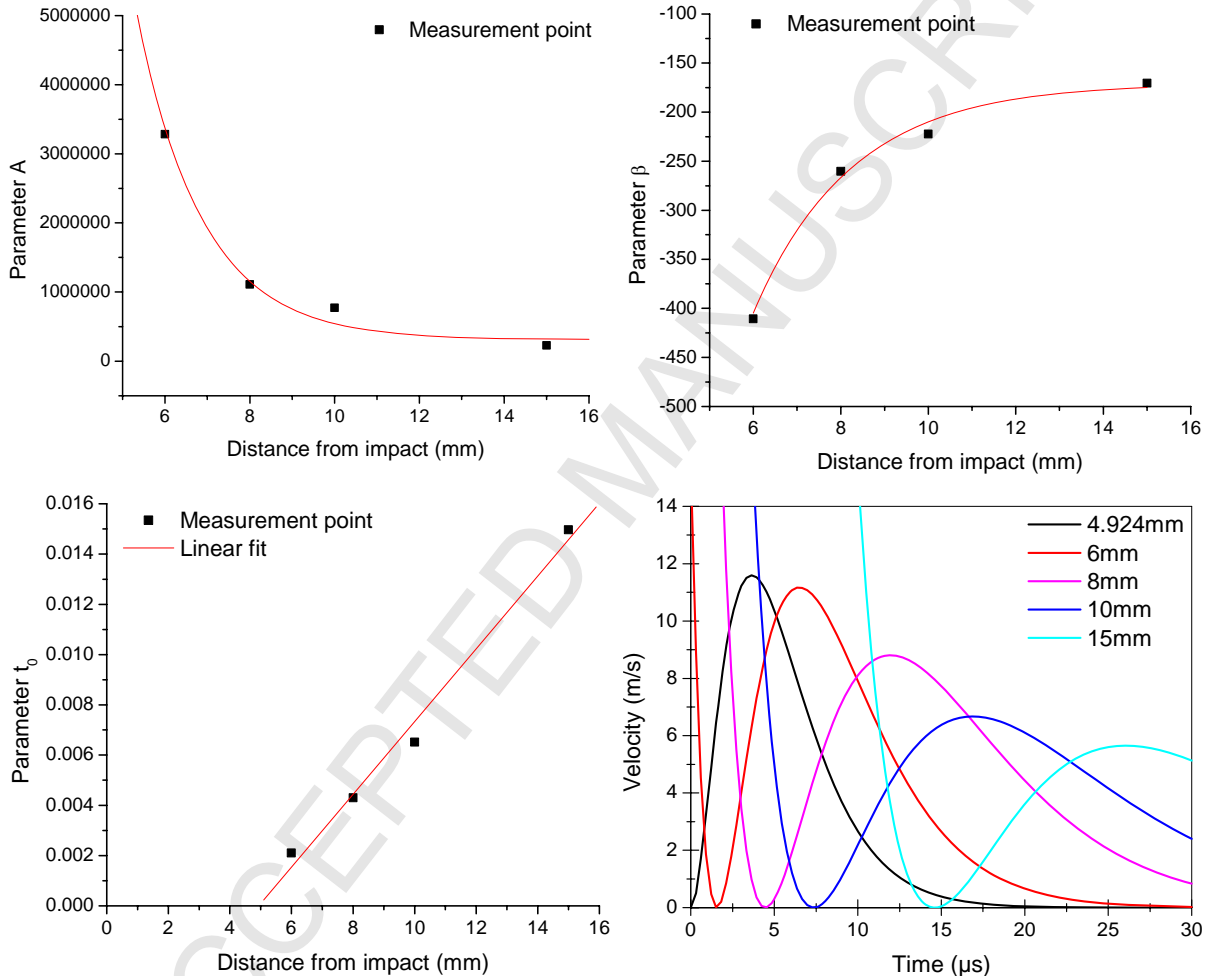


Fig. 6. Characterizing the evolution of the simplified disturbance signal for impact of a 0.6mm Al-sphere at 16.0 km/s and the resulting excitation function (where $x_e = 4.924$ mm)

The excitation area represents, on the rear facesheet, the surface impacted by the expanding fragment cloud. In Fig. 7, fragment cloud expansion is shown to be restricted (or “channeled”) by the presence of the HC cell walls. For this specific case, all fragments are channeled within 2 HC cells.

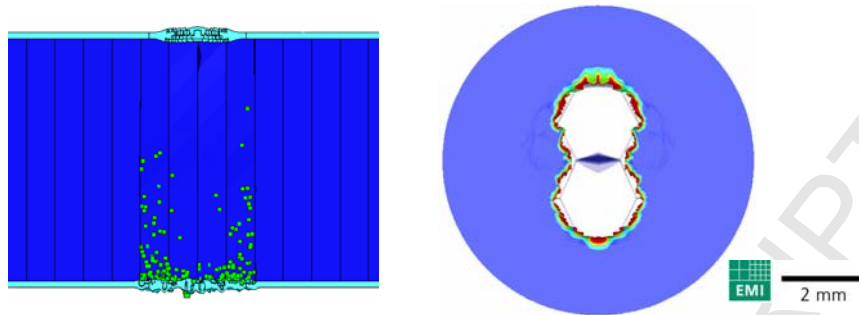


Fig. 7. Channeling of the fragment cloud and the resultant damage on the SP rear facesheet (impact conditions: 0.6mm Al-sphere at 16.0 km/s).

In [10] it was found that for impact of projectiles smaller than the individual honeycomb cells, the degree of channeling is dependant on the specific impact location relative to the honeycomb cells. Although this may be expected to induce different transient disturbances, the primary effect of projectile impact location relative to honeycomb cells walls involves projectile fragmentation and is therefore more relevant in low velocity impacts. As the velocity of debris flux for the GAIA mission ranges from 11 to 72 km/s (with a mean value of 20 km/s) complete fragmentation of the projectile is expected. Thus, the effect of impact location should not be significant. As a default all simulations have been performed with impact to occur directly on the honeycomb cell longitudinal wall.

For the front facesheet the excitation area represents the extension of plastic damage (delamination).

4.1 A General Excitation Function for Impact on the GAIA CFRP/Al HC SP

A general excitation function can be defined which incorporates the effects of projectile diameter and impact velocity on the impact induced-disturbance in terms of the impactor momentum. Considered from an operational standpoint, hypervelocity impacts on the GAIA spacecraft can be classified into three groups, depending on their criticality:

- Low level but frequent impacts leading to a “noise-like” dynamic disturbance. This type of impact concerns particles with an impact frequency higher than one impact per hour;
- Intermediate level and less frequent impacts, which can be considered as discrete events. These impacts lead to a temporary loss of the scientific data and concerns particles with an impact frequency between 1 impact per day and 1 impact per month;
- Rare but high level impacts. Such particles lead to at least to a temporary loss of the mission. These particles have an impact probability lower than 1 impact per year.

The excitation function is concerned only with low and intermediate level impacts, which for the GAIA spacecraft refers to the impact of particles with a mass between $1 \cdot 10^{-11}$ kg and than $1 \cdot 10^{-7}$ kg (for an aluminum sphere this corresponds to projectile diameters between 20 μm and 0.4 mm). In Fig. 8 the ballistic limits of the GAIA SP front and rear facesheets are shown (calculated using equations from [10] and [12] respectively). It can be seen that low and intermediate level impacts cover the four

penetration conditions previously defined. The numerical simulations performed for derivation of the generalized excitation function are also shown in Fig. 8 in terms of the ballistic limit. Simulations are performed with projectiles larger than 0.4 mm due to the validation basis of the numerical model.

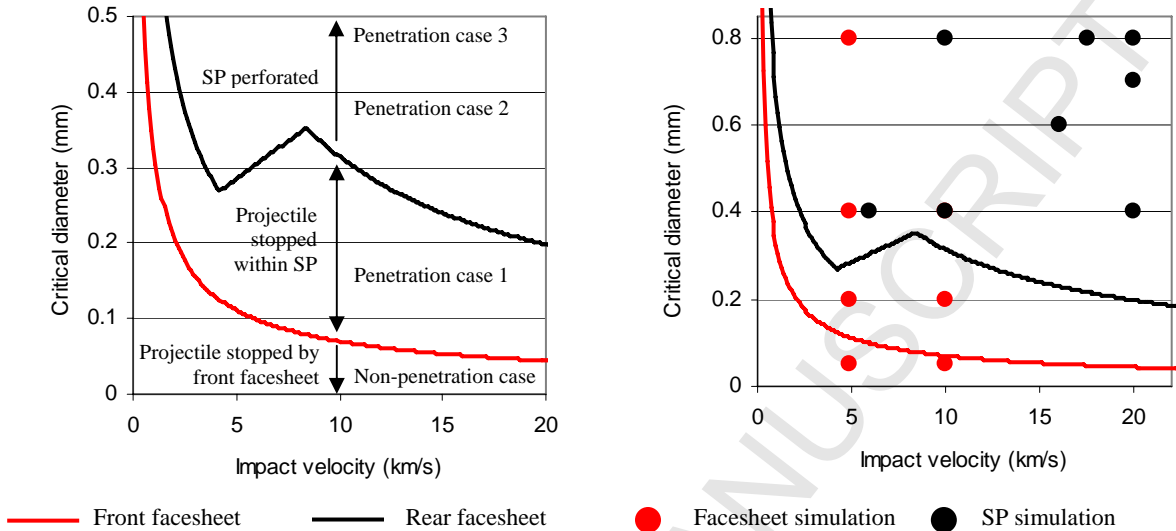


Fig. 8. Ballistic limit curve of the CFRP/Al HC sandwich panel showing front facesheet and sandwich panel perforation limits. Left: four penetration cases; Right: details of the numerical simulations

From the simulations a maximum excitation area radius of 3.765 mm and 4.924 mm was recorded for the front and rear facesheets, respectively. A constant excitation area was thus conservatively defined at 4mm and 6mm for the front and rear facesheets. The rear facesheet excitation function constants determined from the numerical simulations are characterized in Fig. 9 in terms of impactor momentum. The transition from penetration case 2 to case 3 (i.e. reaching and exceeding a level of significant perforation) is defined by the cubic shape of the curves.

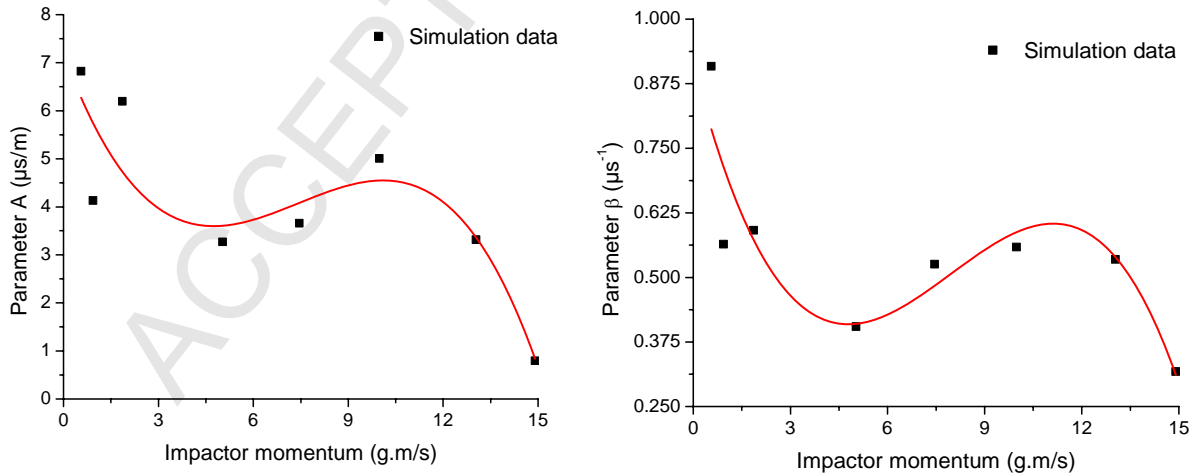


Fig. 9. Characterization of the rear facesheet excitation function constants (solved for $x=6\text{mm}$).

For application of the excitation function in a structural FE code it must be expressed as force with respect to time. The acceleration is determined by taking the time derivative of the velocity excitation function while the excited mass is defined by the area of excitation on the corresponding facesheet. Considering the radius of the excitation area was set as 4 mm and 6 mm for the front and rear facesheet function, the excited mass is calculated as $0.0382 \cdot 10^{-3}$ kg and $0.0597 \cdot 10^{-3}$ kg respectively (0.5 mm thick CFRP facesheets having 1.52 g/cm^3 volumetric density). The front and rear facesheet excitation functions, for application as force with respect to time, are expressed as:

$$F(t) = ma(t) \quad (2)$$

where $a(t) = 2A \cdot t \cdot e^{-\beta \cdot t} - A \cdot t^2 \cdot \beta \cdot e^{-\beta \cdot t}$

Front facesheet	Rear facesheet
$m = 0.0382 \cdot 10^{-3} \text{ kg}$	$m = 0.0860 \cdot 10^{-3} \text{ kg}$
$A = 39.491 - 32.551 \cdot 0.683^{P_p}$	$A = 7.189 - 1.794 \cdot P + 0.278 \cdot P^2 - 0.0125 \cdot P^3$
$\beta = 2.7347 - 0.8494 \cdot P_p + 0.2199 \cdot P_p^2$	$\beta = 0.913 - 0.245 \cdot P + 0.037 \cdot P^2 - 1.54E - 03 \cdot P^3$

The peak excitation force is shown in Fig. 10 for the front and rear facesheet excitation functions. The range of application for the facesheet functions is defined about an impactor momentum of 2.64 g·m/s respectively. This point represents the condition of significant perforation in the front facesheet upon which the majority of momentum transfer changes from the front to rear facesheet. It can be noted that as the impactor momentum approaches zero, the rear facesheet excitation function does not return to the origin. This is due to the rear facesheet excitation function being derived from disturbance signals measured for impact of projectiles with 0.56 g·m/s momentum or higher. Additionally, for impactors with momentum less than $\sim 4.5 \text{ g·m/s}$ there is significant scatter in the fit of the rear facesheet excitation function constants (Fig. 9). Ideally there would be a smooth transition of the peak excitation force of the front facesheet function to the rear facesheet function at the limit of 2.64 g·m/s. It is considered that the current derivation provides conservative solutions in the 2.64-4.5 g·m/s momentum range. The effect of increasing projectile diameter on the induced disturbance waveform is also shown in Fig. 10 for impact at 20 km/s (rear facesheet).

5. Summary and Conclusions

Future generations of European scientific satellites will require platform stability orders of magnitude higher than in previous satellites. In order to quantify the disturbance induced by impact of space debris or meteoroid, a mathematical function has been defined which represents the elastic excitation of a satellite representative structure wall (CFRP/Al HC SP).

ESA's GAIA satellite was selected to quantify the magnitude of disturbances induced by the impact of debris at hypervelocity, and assess the threat this poses on the achievability of mission objectives. GAIA will operate at the Earth-Sun L2 point, an environment dominated by micro-meteoroid particles traveling at velocities in the order of 30-70 km/s. Current hypervelocity acceleration facilities are incapable of reproducing these impact conditions. As such, a campaign of numerical simulations were

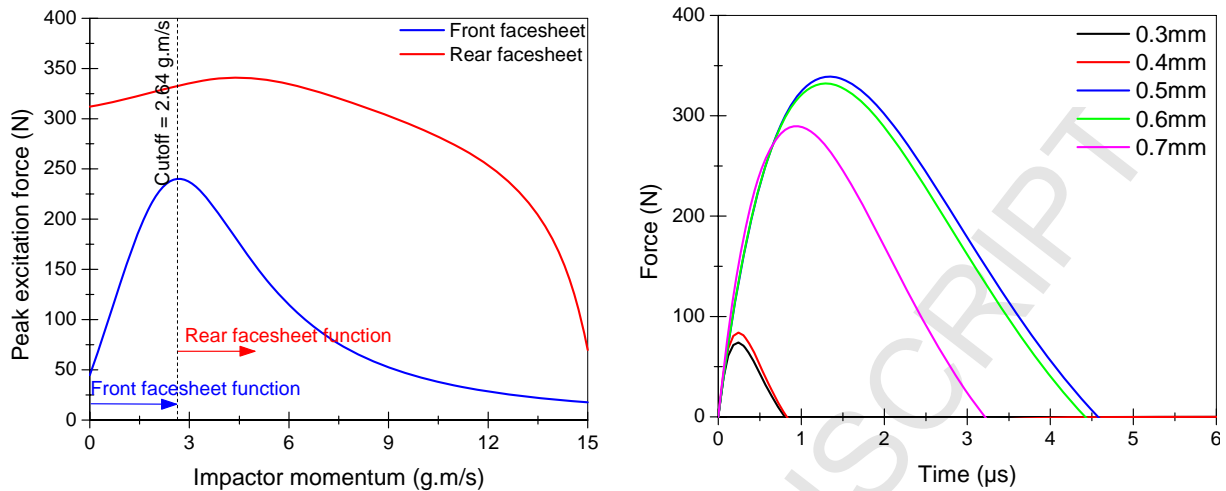


Fig. 10. Generalized excitation function profile. Left: Excitation function profile peak force defined in terms of impactor momentum; Right: Example excitation profiles – the effect of increasing projectile diameter on the induced disturbance (impact velocity = 20 km/s)

performed using the commercial hydrocode AUTODYN in which the local impact-induced transient waves were measured and key features of the signal (i.e. flexural wave) were characterized. The simulation measurements were validated through comparison with experimental signals at achievable impact conditions (1.5mm Al-sphere at ~ 5.70 km/s), recorded using an effectively mass-less laser interferometer (laser vibrometer). Good qualitative agreement was found between the two signals, and sufficient reproduction of the flexural wave characteristics was observed.

Given the range of impact conditions relative to the GAIA mission (impactor mass, impact velocity), a general excitation function has been derived which accounts for the impact parameters in terms of momentum. This generalized function, expressed in two parts (front- and rear facesheet) allows the derivation of an excitation function for any combination of impactor diameter and velocity within the range of validity (max projectile diameter 0.8mm).

For implementation of the excitation function in global satellite finite element models, the impact excitation is expressed as force in terms of time. Furthermore, the area and mass of the relevant facesheet subject to acceleration is defined to ensure consistency between the numerical methods (hydrocode, FE packages).

Application & Further Work

The excitation function has been applied in a full-scale FE model of the GAIA satellite in [1]. It is shown that the methodology proposed within this paper for characterization of the transient disturbance induced by hypervelocity impact on CFRP/Al HC SPs is suitable for application and quantification of disturbance magnitudes.

The goal of this work was the development of a suitable procedure for disturbance characterization.

For use in M/SD risk analysis, additional confidence is required in the characterization procedure. The numerical disturbance signal was found to be highly sensitive to the material EOS parameters. However, it is not certain that experimental characterization of these parameters will result in an improved model (given limitations of the EOS model in the advanced orthotropic composite material model of [2][3]). Experimental validation over a broader range of impact conditions (smaller projectiles, higher velocities) would give more confidence in the numerical model. Furthermore, an additional validation loop in which the elastic excitation signal is applied in the hydrocode model and compared to the evolution of the impact-induced waveform could also be considered.

Acknowledgements

Sections of this work have been performed as part of ESA Contract 18583 “Spacecraft Disturbances from Hypervelocity Impact”.

References

- [1] Guyot M, Vergniaud J, Lambert M, Schaefer F, Ryan S, Hiermaier S, Taylor E. Structural vibrations induced by HVI – application to the GAIA spacecraft. HVIS, 2007.
- [2] Clegg R, White D, Riedel W, Harwick W. Hypervelocity impact damage prediction in composites: Part I – material model and characterization. *International Journal of Impact Engineering* 2006; **33**(1-2): 190-200.
- [3] Riedel W, Nahme H, White D, Clegg R. Hypervelocity impact damage prediction in composites: Part II – material model and characterization. *International Journal of Impact Engineering* 2006; **33**(1-2): 670-680.
- [4] Wicklein M, Ryan S, White D, Clegg R. Hypervelocity impact on CFRP: testing, material modelling, and numerical simulation. HVIS, 2007.
- [5] Century Dynamics Inc. AUTODYN Theory Manual – Revision 4.3. Concord, USA, 2005.
- [6] Ryan S, Wicklein M, Riedel W, Schaefer F, Thoma K. Theoretical prediction of dynamic composite material properties for numerical simulation. For submission to *Composites, Science and Technology*, 2007.
- [7] Stilp A. Review of modern hypervelocity impact facilities. *International Journal of Impact Engineering*, 1987; **5**: 613-621.
- [8] Schaefer F, Putzar R. Spacecraft Disturbances from Hypervelocity Impact–Impact Testing. WP4000 of ESA Contract 18585, FhG Ernst- Mach- Institut (EMI), Report I-09/07, Freiburg, Germany.
- [9] Ryan S, Schaefer F, Spencer G, Hiermaier S, Guyot M, Lambert M. An excitation function for hypervelocity impact-induced wave propagation in satellite structures. 57th IAC, Oct. 2-6 2006, Valencia.
- [10] Ryan S, Riedel W, Schaefer F. Numerical study of hypervelocity space debris impacts on CFRP/Al honeycomb spacecraft structures. 55th IAC, Oct. 4-8 2004, Vancouver.
- [11] Schaefer F, Schneider E, Lambert M. Review of ballistic limit equations for CFRP structure walls of satellites. 5th Int. Symp. on Env. Testing for Space Programmes, ESA SP-558, June 15-17 2004, Noordwijk.
- [12] Ryan S, Schaefer F, Destefanis R, Lambert M. A ballistic limit equation for hypervelocity impacts on CFRP/Al HC satellite structures. *Advances in Space Research*, 2007; In Corrected Proof.

APPENDIX

CFRP Facesheets: M55J/XU3508 (hardener 3473)

Parameter	Value	Parameter	Value	Parameter	Value
Equation of State: Ortho		Strength: Orthotropic Yield		Failure: Orthotropic Softening	
Reference density	1.52 g/cm ³	A11 []	1	Ten. Failure Stress 11	161.20 MPa
Young's Mod. 11	23.64 GPa	A22 []	0.1484	Ten. Failure Stress 22	208.41 MPa
Young's Mod. 22	49.12 GPa	A33 []	0.5979	Ten. Failure Stress 33	208.50 MPa
Young's Mod. 33	5.98 GPa	A12 []	-0.0615	Max. Shear Stress 12	130.10 MPa
Poisson's Ratio 12	0.054	A13 []	0	Max. Shear Stress 23	60.376 MPa
Poisson's Ratio 23	0.421	A23 []	-0.0625	Max. Shear Stress 31	60.376 MPa
Poisson's Ratio 31	0.0085	A44 []	2.726	Fracture Energy 11	1E-06 J/m ²
Shear Modulus 12	14.88 GPa	A55 []	2.726	Fracture Energy 22	1E-06 J/m ²
Shear Modulus 23	2.86 GPa	A66 []	0.2647	Fracture Energy 33	420 J/m ²
Shear Modulus 31	2.86 GPa	Eff. Stress #1	115.93 MPa	Fracture Energy 12	1360 J/m ²
Bulk Modulus A1	10.22 GPa	Eff. Stress #2	128.64 MPa	Fracture Energy 23	1E-06 J/m ²
Parameter A2	6.88 GPa	Eff. Stress #3	141.35 MPa	Fracture Energy 31	1E-06 J/m ²
Parameter A3	6.85 GPa	Eff. Stress #4	154.05 MPa		
Parameter B0	1.996	Eff. Stress #5	162.77 MPa		
Parameter B1	1.996	Eff. Stress #6	171.03 MPa		
Parameter T1	20.33 GPa	Eff. Stress #7	178.76 MPa		
Parameter T2	6.88 GPa	Eff. Stress #8	184.99 MPa		
		Eff. Stress #9	191.23 MPa		
		Eff. Stress #10	197.46 MPa		
		Eff. Pl. Stn. #1	0		
		Eff. Pl. Stn. #2	2.54E-04		
		Eff. Pl. Stn. #3	5.09E-04		
		Eff. Pl. Stn. #4	7.63E-04		
		Eff. Pl. Stn. #5	0.00102		
		Eff. Pl. Stn. #6	0.00127		
		Eff. Pl. Stn. #7	0.00153		
		Eff. Pl. Stn. #8	0.00178		
		Eff. Pl. Stn. #9	0.00204		
		Eff. Pl. Stn. #10	0.00229		

Honeycomb Core: Al 5056

ρ [g/cm ³]	K [GPa]	T_{ref} [K]	c [J/kgK]	G [GPa]	A [MPa]	B [MPa]	n [-]	C [-]	m [-]	$\dot{\epsilon}_{ref}$ [s ⁻¹]	ϵ_{pl} [-]
2.780	79.06	293.0	875.0	27.6	140.0	426.0	0.34	0.015	1.00	1.00	0.70

Projectile: Al 2017-T4

ρ [g/cm ³]	Γ [-]	CI [m/s]	SI [-]	T_{ref} [K]	c [J/kgK]	G [GPa]	A [MPa]	B [MPa]	n [-]	C [-]	m [-]	$\dot{\epsilon}_{ref}$ [s ⁻¹]	ϵ_{pl} [-]
2.780	2.0	5328	1.338	293	875.0	27.6	140.0	426.0	0.34	0.015	1.0	1.0	0.70